Food Hydrocolloids 170 (2026) 111773

Contents lists available at ScienceDirect

Food Hydrocolloids

journal homepage: www.elsevier.com/locate/foodhyd

Interfacial engineering through chitin retention unlocks the emulsification potential of *Fusarium venenatum* mycoprotein

Yingying Jin [a,b,c], Hanyun Jiang [a,b], Guocheng Du [a,b,c], Jian Chen [a,b,c,*], Zhitong Zhou [a,b,c,**], Xiao Liu [a,b,c,***]

[a] Science Center for Future Foods, Jiangnan University, Wuxi, 214122, China
[b] Jiaxing Institute of Future Food, Jiaxing, 314000, China
[c] School of Biotechnology, Jiangnan University, Wuxi, 214122, China

ARTICLE INFO

Keywords:
Fusarium venenatum mycoprotein
Chitin
Interfacial engineering
Dilatational rheology
Emulsion stability

ABSTRACT

Fusarium venenatum represents a nutritionally rich and sustainable mycoprotein (MP) source with considerable promise for functional food development. However, its 'chitin-glucan' cell wall architecture restricts interfacial migration of intracellular proteins. While conventional physical disruption effectively reduced β-glucan content, chitin degradation remained limited. To specifically assess the critical role of chitin in modulating MP interfacial functionality, chitinase was employed to generate chitinase-treated mycoprotein (CMP). Remarkably, chitin removal enhanced protein solubility by 106.7% and surface hydrophobicity by 68.7%. Interfacial engineering analysis was performed to elucidate how residual chitin governs the emulsifying performance of MP. The adsorption kinetics at the oil-water interface indicated that MP and CMP formed interfaces with significantly lower interfacial tension than conventional protein emulsifiers soy protein (SP) or whey protein (WP). Critically, interfacial rheological measurements demonstrated that MP, due to the presence of residual chitin, exhibited superior deformation resistance compared to CMP. Moreover, Lissajous plots and S-factors demonstrated more pronounced strain softening behavior in MP, indicating its interfacial film possesses greater repair capability. Furthermore, MP- and CMP-stabilized emulsions exhibited similar droplet size, which were significantly smaller than those of SP and WP. Notably, MP-stabilized emulsions demonstrated superior stability compared to CMP, while performing comparably to WP-based systems. These results revealed that residual chitin in MP acted as a natural interfacial modifier, synergistically interacting with proteins to enhance interfacial film mechanical strength and emulsion stability. This study reveals the exceptional emulsification potential of *F. venenatum* mycoprotein, positioning it as a highly promising, sustainable alternative to conventional protein emulsifiers.

1. Introduction

Global population growth has driven a surge in protein demand, yet conventional production methods remain inefficient (Pastrana-Pastrana et al., 2025). Humans urgently needed to explore efficient and sustainable alternative proteins. (Puljić et al., 2025). *Fusarium venenatum* is a mycoprotein (MP) source approved for human consumption by regulatory agencies including the Food and Drug Administration and European Food Safety Authority (Ahmad et al., 2022; Derbyshire & Ayoob, 2019). Recognized as a promising alternative protein, it exhibits meat-like sensory attributes, high production efficiency, and a nutritionally complete profile (Wood & Tavan, 2022). Nevertheless, MP is encapsulated by a rigid 'chitin-glucan' cell wall, which is a polysaccharide outer wall that inhibits the hydration capacity and interfacial migration activity of intracellular proteins (Garcia-Rubio et al., 2020). This limits its application in emulsion food systems. Therefore, breaking down the cell wall structure and developing efficient protein extraction techniques are crucial for advancing the use of MP in liquid systems.

Current cell wall disruption strategies include bead milling, high-pressure homogenization, ultrasonication, and enzymatic lysis. Notably, Zeng et al. (2023) demonstrated that high-pressure homogenization coupled with pH-shifting achieved superior cell wall removal

* Corresponding author. Science Center for Future Foods, Jiangnan University, Wuxi, 214122, China.
** Corresponding author. Science Center for Future Foods, Jiangnan University, Wuxi, 214122, China.
*** Corresponding author. Science Center for Future Foods, Jiangnan University, Wuxi, 214122, China.
E-mail addresses: jchen@jiangnan.edu.cn (J. Chen), zzhou@jiangnan.edu.cn (Z. Zhou), liuxiao@jiangnan.edu.cn (X. Liu).

https://doi.org/10.1016/j.foodhyd.2025.111773
Received 13 June 2025; Received in revised form 9 July 2025; Accepted 16 July 2025
Available online 16 July 2025

efficiency compared to individual enzymatic or ultrasonic treatments. However, chitin is predominantly localized in the inner cell wall layer (Garcia-Rubio et al., 2020), making complete removal difficult through physical methods alone. Previous studies confirmed that polysaccharides could interact with proteins, thereby modifying interfacial and emulsion properties. For example, Ma et al. (2025) systematically demonstrated that diverse polysaccharides modulate protein interfacial behavior differently through specific molecular interactions. Similarly, Wang et al. (2020) demonstrated that chitin nanofibrils-protein interactions enhanced emulsion stability, whereas excessive chitin nanofibrils induced protein aggregation and subsequent flocculation. To investigate the effects of residual chitin on the oil-water interfacial and emulsifying properties of MP, this study introduced chitinase to specifically hydrolyze chitin in the MP.

Interfacial engineering was employed to systematically evaluate the properties of oil-water interfaces. During emulsion formation, proteins migrate from the aqueous phase to the oil-water boundary and structural reorganization (Cai et al., 2025). This interfacial behavior under static conditions can be quantitatively monitored through interfacial adsorption kinetics (García-Moreno et al., 2021). However, during emulsion processing, the interface is often subjected to external disturbances and exhibits significant deformation. To accurately assess the nonlinear viscoelastic properties of interfacial layers, large-amplitude oscillatory dilatational rheology becomes essential (Sagis & Fischer, 2014; Yang et al., 2024). Quantitative analysis of interfacial film nonlinear responses under oscillatory and large shear deformations via Lissajous plots and S-factors calculations enables more accurate determination of interfacial characteristics (Zhan et al., 2020). For instance, Wen et al. (2024) employed interfacial shear and spreading rheology to demonstrate that protein film viscoelasticity governed droplet stability. Romero et al. (2011) revealed that highly elastic interfacial films resist rupture caused by droplet collisions, thereby enhancing long-term emulsion stability. These findings demonstrated that oil-water interfacial rheology can serve as an effective indicator of emulsion stability and functionality, highlighting the need for further investigation into the interfacial properties of MP.

This study focused on analyzing the physicochemical properties of MP extracted from *F. venenatum* and chitinase-treated mycoprotein (CMP), which underwent specific chitin hydrolysis. The key physicochemical properties assessed encompassed solubility, particle size, ζ-potential, surface hydrophobicity, and interfacial engineering. The emulsion stabilization capacity was assessed through interfacial adsorption kinetics and dilatational rheology measurements at oil-water interfaces. Comparative analysis with conventional soy protein (SP) and whey protein (WP) was conducted to establish a foundation for the advanced utilization of MP in the food industry.

2. Materials and methods

2.1. Materials

F. venenatum was obtained from Jiangxi Fushine Biotechnology Co. (Jingdezhen, China), WP was purchased from Jiangsu Puxing Biotechnology Co. (Nanjing, China), and SP was extracted according to the method of Wen et al. (2024). Chitinase was purchased from Shanghai Macklin Biochemical Co. (Shanghai, China). Sunflower oil was purchased from a local supermarket and purified using Florisil (60–100 mesh, Sigma-Aldrich, Saint Louis, USA). Ultrapure water (Milli-Q Purelab Ultra, Darmstadt, Germany) was used for all experiment.

2.2. Extraction of proteins

2.2.1. Extraction of mycoprotein (MP)

Fusarium venenatum MP was extracted through high-pressure homogenization coupled with alkaline extraction and isoelectric precipitation. Briefly, *F. venenatum* biomass was homogenized in water (1:25, w/v) at 12,000 rpm for 5 min using an IKA T25 digital Ultra-Turrax (IKA Works, Wilmington, USA) while maintaining pH at 12.0 with 1 M NaOH. The suspension was left undisturbed overnight and then homogenized using a Nano DeBEE high-pressure homogenizer (BEE International, San Diego, USA) at 120 MPa for two cycles. After centrifugation (8000 rpm, 15 min), the supernatant was acidified to pH 4.5 with 1 M HCl, stirred for 30 min, and centrifuged again. The precipitated proteins were resuspended in water, neutralized to pH 7.0, and dialyzed (8.0 kDa MWCO membrane, 48 h). Finally, the retentate was freeze-dried to obtain purified MP.

2.2.2. Extraction of chitinase-treated mycoprotein (CMP)

The MP was homogenized with distilled water at a ratio of 1:10 (w/v) under continuous stirring at 37 °C for 1 h. Chitinase was then added to the mixture at a concentration of 5 U/g (enzyme to substrate ratio) for enzymatic hydrolysis at 37 °C. After 2 h of incubation, the pH was adjusted to 4.5, followed by centrifugation to collect the protein precipitate. The obtained precipitate was uniformly dispersed in water, adjusted to pH 7.0, then dialyzed and freeze-dried to obtain CMP.

2.3. Determination of protein content

Protein content was determined in triplicate using a K9860 fully automated Kjeldahl nitrogen analyzer (Hanon, Jinan, China). The nitrogen conversion factor was 6.25.

2.4. Determination of chitin content

The sample (5 mg) was dissolved in 1 mL of 6 M HCl and incubated at 100 °C for 17 h. The mixture was dried and subsequently reconstituted in 1 mL water, followed by centrifugation at 8000 rpm for 10 min. 0.1 mL supernatant was mixed with 0.1 mL Solution A (1.5 mol Na_2CO_3 in 4% (v/v) acetylacetone), water bath heating (100 °C, 20 min). Then added with 0.7 mL 95% ethanol and 0.1 mL Solution B (1.6 g of p-dimethylaminobenzaldehyde dissolved in 30 mL of 12 M HCl and 30 mL of 95% ethanol). After 1 h incubation, absorbance at 520 nm was measured (N-acetylglucosamine standard). Chitin content was expressed as the percentage of glucosamine relative to the sample weight.

2.5. Determination of β-glucan content

The β-glucan content was determined using the Mushroom and yeast beta-glucan assay Kit (Megazyme, Ireland). This method was based on the enzymatic hydrolysis of β-glucans into glucose by exo-1,3-β-glucanase and β-glucosidase. The released glucose was then specifically oxidized in the presence of glucose oxidation-peroxidase buffer reagent, generating a pink-colored product. Measured the absorbance at 510 nm using D-glucose as the standard. The β-glucan content was expressed as the percentage of D-glucose to the sample weight.

2.6. Physicochemical properties of proteins

2.6.1. Protein solubility

A 5 mg/mL neutral protein solution was centrifuged (3000 rpm, 3 min), and the supernatant protein concentration was measured by BCA assay kit (Beyotime, Shanghai, China). Protein solubility was expressed as the percentage of soluble protein concentration relative to total protein concentration.

2.6.2. ζ-potential

The ζ-potential of a 1 mg/mL protein solution (pH 7.0) was measured using a Zetasizer Nano ZS (Malvern Instruments Ltd., UK). The dispersed phase was water with a refractive index of 1.33, and the continuous phase was 1.45. All measurements were performed at 20 °C.

2.6.3. Surface hydrophobicity (H_0)

The 10 mg/mL neutral protein solution was centrifuged at 3000 rpm for 3 min, and the supernatant was diluted to 0.1–0.5 mg/mL. Measure the fluorescence intensity (FI_0) of 3 mL of the diluted solution at excitation/emission wavelengths of 370/465 nm. After adding 20 μL of 8-anilino-1-naphthalenesulfonic acid (ANS), FI_1 was measured immediately. Surface hydrophobicity was quantified as the regression slope of ΔFI (FI_1 - FI_0) against protein concentration.

2.7. Oil-water interface characterization of proteins

2.7.1. Interfacial adsorption

Protein adsorption kinetics at the oil-water interface were analyzed with an LSA 100 optical surface analyzer (LAUDA Scientific, Lauda-Königshofen, Germany). A 20 μL droplet of 1 mg/mL neutral protein solution was held in purified sunflower oil via a syringe. Continuously calculated the interfacial tension at 25 °C for 3 h.

2.7.2. Interfacial expansion rheology

Droplet were equilibrated for 3 h prior to measurement. The interfacial elastic modulus (E_d') and viscous modulus (E_d'') during scanning were calculated through Fourier transform analysis. Frequency sweeps were performed from 0.005 Hz to 0.1 Hz at a fixed amplitude of 5%, and the exponent n was calculated using a power function model ($E_d' \sim \omega^n$, ω was the frequency). Amplitude sweeps was swept from 5% to 30% at a fixed frequency of 0.01 Hz. Frequency sweeps and Amplitude sweeps amplitudes both perform 5 cycles.

2.7.3. Lissajous plot

The Lissajous plot was constructed based on the surface pressure (Π = γ-γ_0, where γ was the surface tension of area, γ_0 was the surface tension of the initial interface) and the surface deformation ($\delta A/A_0$, where $\delta A = A\text{-}A_0$, A was the deformed interface area, and A_0 was the initial interface area). The S-factors for the expansion and compressive stages was calculated by the following (Sagis & Fischer, 2014):

$$S_{ext} = \frac{E_{L,E} - E_{M,E}}{E_{L,E}} \quad (1)$$

$$S_{com} = \frac{E_{L,C} - E_{M,C}}{E_{L,C}} \quad (2)$$

where $E_{L,E}$, $E_{M,E}$ denote the larger and smallest strain moduli in expansion, $E_{L,C}$ and $E_{M,C}$ denote the largest and smallest strain moduli in compression.

2.8. Emulsification capacity

2.8.1. Emulsion preparation

The protein was dissolved in water to obtain a 0.5% (w/v) neutral solution, which was then mixed with sunflower oil at a 9:1 (v/v) ratio. The mixture was pre-homogenized at 1200 rpm for 2 min using an IKA T25 digital Ultra-Turrax homogenizer (IKA Works, Wilmington, USA), followed by high-pressure homogenization at 100 MPa to prepare the protein emulsion. The final emulsion was supplemented with 0.1% (w/w) Bit 10 bacteriostat to prevent microbial growth and stored at 4 °C.

2.8.2. Droplet size and ζ-potential

The particle size ($d_{4,3}$) of emulsion droplets was monitored continuously for 30 d using a Mastersizer 3000E (Malvern Instruments Ltd., UK). The emulsion was diluted 100 fold with water, and the ζ-potential was measured using a Zetasizer Nano ZS. The particle phase and dispersant were purified sunflower oil and water, with refractive indices of 1.47 and 1.33, respectively.

2.8.3. Adsorbed proteins of emulsions

The prepared emulsion was centrifuged at 100,000 rpm for 30 min at 4 °C using an ultracentrifuge (CP100NX, Himac, Japan). The aqueous phase was filtered through a 0.22 μm membrane. The protein concentration of the filtrate was then determined. The absorbed protein percentage (AP) and interfacial protein concentration (Γ) were calculated as follows:

$$AP\ (\%) = \frac{C_0 - C_S}{C_0} \times 100 \quad (3)$$

$$\Gamma(mg/m^2) = \frac{(C_0 - C_S)(1-\varphi)d_{3,2}}{0.6} \quad (4)$$

where c_0 is the protein concentration in the emulsion, c_s is the protein concentration in the aqueous phase, and $d_{3,2}$ is the volume-surface average diameter of emulsion.

2.8.4. pH stability of emulsions

The pH of freshly stabilized emulsions was adjusted to 3.0–7.0 and stored at 4 °C for 24 h. Droplet size was measured to evaluate pH-dependent emulsion stability.

2.9. Statistical analysis

All tests were conducted in triplicate. Data are reported as mean ± standard deviation. Significant differences were analyzed by one-way ANOVA (IBM SPSS 25.0), with Duncan's post hoc test ($p < 0.05$) for multiple comparisons.

3. Results and discussion

3.1. Content of protein and cell wall components

Compared to *F. venenatum* biomass, both MP and CMP exhibited significant alterations in protein content and cell wall components (Fig. 1). The disruption of *F. venenatum* cell walls released intracellular proteins, elevating the protein content from 47.84% in the biomass to 74.03% in MP. Concurrently, the β-glucan content decreased dramatically, demonstrating effective removal of β-glucans from the cell walls. In contrast, the chitin content decreased only slightly, revealing the limited effectiveness of mechanical processing alone for chitin breakdown. This phenomenon may be attributed to chitin's localization within the inner cell wall layers and its capacity to form stable complexes with proteins through electrostatic interactions and hydrogen bonding (Garcia-Rubio et al., 2020; Yu et al., 2014). However, when MP was treated with chitinase to specifically hydrolyze chitin, the resulting CMP demonstrated a substantial reduction in chitin content to 2.86%, along with a remarkable increase in protein content to 80.74%.

3.2. Colloidal properties

The colloidal properties of the individual proteins are summarized in Table 1. Chitin removal through enzymatic treatment substantially enhanced the fundamental properties of CMP compared to MP. Chitinase mediated specific hydrolysis of positively charged chitin in MP exposed additional negatively charged carboxyl groups (particularly glutamic acid and aspartic acid residues) on the protein surface, consequently increasing the surface charge of the CMP solution to −32.36 mV. Meanwhile, CMP demonstrated a significantly smaller particle size than MP, suggesting that chitin removal induced protein conformational changes and reduced intermolecular aggregation (Tavares et al., 2021). Notably, CMP exhibited significantly higher solubility than MP, which can be attributed to enhanced electrostatic repulsion between protein molecules due to the increased surface charge. This effect overcome aggregation driven by van der Waals forces, thereby improving colloidal stability (Malhotra & Coupland,

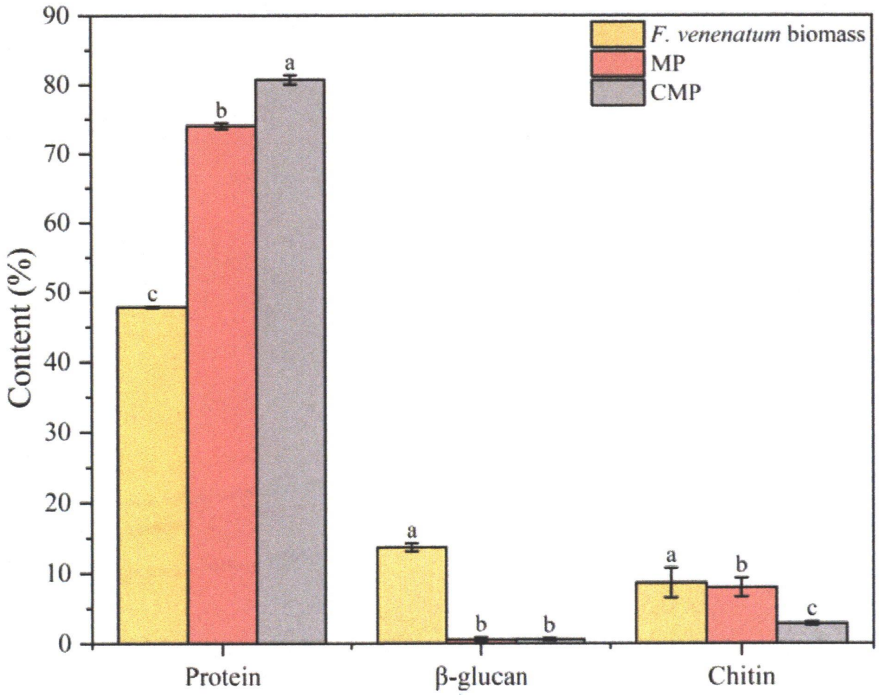

Fig. 1. Protein, β-glucan, and chitin content (%) of *F. venenatum* biomass, mycoprotein (MP) and chitinase-treated mycoprotein (CMP).

Table 1
Particle size, ζ-potential, solubility and surface hydrophobicity of mycoprotein (MP), chitinase-treated MP (CMP), soy protein (SP) and whey protein (WP).

	MP	CMP	SP	WP
Protein size (nm)	274.73 ± 5.10^{a}	224.20 ± 7.02^{b}	127.23 ± 0.33^{d}	191.93 ± 0.14^{c}
ζ-potential (mV)	−28.79 ± 0.03^{b}	−32.36 ± 1.45^{c}	−32.95 ± 0.67^{c}	−20.51 ± 0.43^{a}
Solubility (%)	39.91 ± 0.27^{d}	82.47 ± 0.79^{c}	93.24 ± 1.43^{a}	88.64 ± 0.38^{b}
Surface hydrophobicity	371.25 ± 7.83^{c}	286.17 ± 17.23^{d}	393.72 ± 33.89^{b}	664.58 ± 30.09^{a}

2004). Additionally, the reduced particle size likely contributed to the solubility enhancement by increasing the protein-solvent interfacial area (Yang et al., 2024). Among the tested proteins, SP exhibited the highest solubility, which correlated with its smallest particle size and most pronounced ζ-potential. In contrast, WP maintained considerable solubility owing to its intrinsic hydrophilic surface properties (Ryan et al., 2012).

The surface hydrophobicity profiles of various proteins at pH 7.0 were illustrated in Table 1. Notably, CMP demonstrated the highest surface hydrophobicity, showing a striking 69% enhancement compared to MP. This pronounced difference implied that residual chitin in MP potentially formed electrostatic complexes with hydrophobic protein regions, thereby shielding these domains from ANS probe accessibility (Ma et al., 2024). Conversely, chitin elimination in CMP appeared to trigger protein structural reorganization, leading to the re-exposure of previously concealed hydrophobic moieties and consequent amplification of surface hydrophobicity (Liu et al., 2022; Ma et al., 2025). WP exhibited the lowest hydrophobicity index which could be attributed to WP's densely packed tertiary structure in aqueous solution, which effectively restricted ANS probe access to its internal hydrophobic domains.

3.3. Oil-water interface adsorption behavior

The temporal evolution of interfacial tension at the oil-water interface by different proteins was presented in Fig. 2. The adsorption phase consisted of two distinct stages (Cai et al., 2025; Romero et al., 2011). During the initial stage (0–500 s), the interfacial tension decreased exponentially, reflecting continuous adsorption of proteins at the oil-water interface. In the subsequent stage (>500 s), the interfacial tension decreased gradually with prolonged adsorption time, suggesting structural reorganization of the proteinaceous interfacial film. MP and CMP displayed markedly faster adsorption kinetics during the initial phase, as demonstrated by their significantly steeper interfacial tension reduction rates relative to SP and WP. After 3 h equilibration, pronounced differences in final interfacial tension emerged, with MP-stabilized interfaces maintaining higher interfacial tension (10.34 mN/m) than CMP (9.30 mN/m). These interfacial characteristics correlated directly with the surface hydrophobicity profiles depicted in Table 1. Upon removal of chitin from CMP, a substantial number of hydrophobic domains became exposed on the protein surface. This structural change promoted protein diffusion toward the oil-water interface and significantly enhanced adsorption efficiency, leading to a faster and more pronounced reduction in interfacial tension (Schröder et al., 2017). In contrast, interfaces stabilized by SP and WP reached higher equilibrium interfacial tension values (10.96 mN/m and 11.56 mN/m, respectively), consistent with their lower surface hydrophobicity.

3.4. Oil-water interfacial dilatational rheology

3.4.1. Frequency sweeps

The mechanical characteristics of protein-stabilized oil-water interfacial films were systematically examined through interfacial dilatational rheology. In the frequency sweep experiments, the deformation amplitude was maintained at 5% (Fig. 3A). The elastic modulus (E_d')

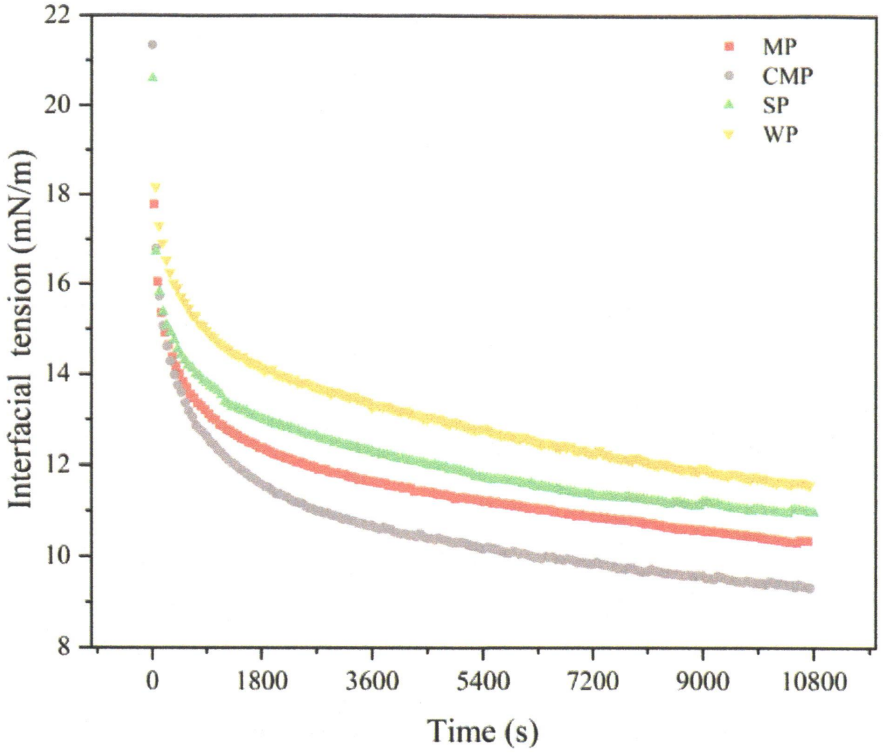

Fig. 2. Interfacial tension of the oil-water interfaces stabilized by mycoprotein (MP), chitinase-treated mycoprotein (CMP), soy protein (SP) and whey protein (WP).

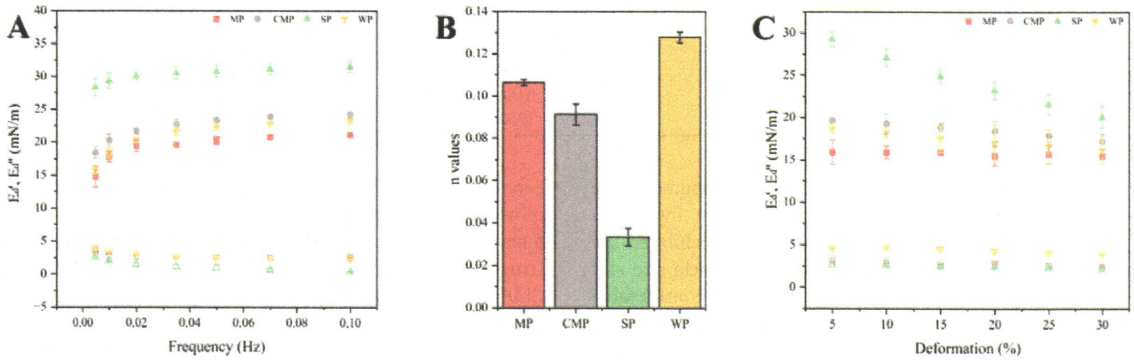

Fig. 3. (A) Frequency dependence of elastic modulus (E_d') and viscous modulus (E_d") at a fixed strain amplitude of 5% for oil-water interfaces stabilized by mycoprotein (MP), chitinase-treated MP (CMP), soy protein (SP), and whey protein (WP). (B) Power-law index (n) derived from frequency sweep measurements. (C) Amplitude dependence of E_d' and E_d" at a fixed frequency of 0.01 Hz. Closed symbols indicate E_d' and hollow symbols indicate E_d".

consistently exceeded the viscous modulus (*Ed*") throughout the tested frequency range, confirming predominantly elastic behavior within the linear viscoelastic (LVE) regime. Concurrently, E_d' exhibited distinct viscoelastic responses as a function of frequency. At lower frequencies, interfacial protein molecules exhibited viscous characteristics due to adequate time for structural reorganization, while higher frequencies induced faster deformation adaptation, resulting in enhanced elastic responses (Zhan et al., 2020). The frequency dependence of the interface was evaluated by calculating the exponent n through the function model ($E_d' \sim \omega^n$). The results shown in Fig. 3B revealed that n values ranged from 0.034 to 0.128 for all samples, with values significantly lower than 0.5. These findings, consistent with Lucassen-van den Tempel model predictions, suggested limited protein exchange between the interface and bulk phase during oscillatory deformation, indicative of a viscoelastic solid-like interfacial architecture (Li et al., 2021). Notably, CMP-stabilized interfaces demonstrated superior elastic properties (elevated E_d' and reduced n values) compared to MP-stabilized interfaces under small deformations, underscoring the positive impact of chitin removal on interfacial rigidity (Wen et al., 2024). In contrast, SP showed the highest E_d' values and n values closest to 0 across all frequencies, while WP demonstrated the largest n value (Ma et al., 2024).

3.4.2. *Amplitude sweeps*

The amplitude sweep was performed at a fixed frequency of 0.01 Hz (Fig. 3C). All protein-stabilized interfaces displayed progressive reduction in E_d' with increasing deformation amplitude while remaining consistently higher than the E_d'', demonstrating progressive disruption of interfacial microstructure while preserving solid-like characteristics (Romero et al., 2011). Notably, at 5% strain, MP-stabilized interfaces exhibited significantly lower E_d' (15.89 mN/m) compared to CMP (19.63 mN/m), demonstrating that chitin removal enhanced interfacial membrane flexibility. However, under large deformation (30% strain),

MP-stabilized interfaces demonstrated superior structural integrity with merely 2.84% E_d' reduction, contrasting sharply with the 12.63% decrease observed for CMP. This indicated that although the MP-stabilized interface showed lower initial stiffness, it exhibited superior resistance to structural disruption under increasing deformation amplitudes, maintaining greater mechanical stability throughout the deformation process (Yang et al., 2024). The improved strain resistance likely arose from interactions between residual chitin and proteins in MP, which facilitated the formation of disordered protein structures (Xiong et al., 2025). This structural modification enhanced the flexibility and adaptability of MP, thereby improving the extensibility of the MP-stabilized interface (Ma et al., 2025). Concurrently, WP-stabilized interfaces maintained comparable flexibility to MP throughout the testing regime. In contrast, SP-stabilized interfaces demonstrated limited mechanical adaptability, as evidenced by a substantial 31.50% reduction in E_d' values despite exhibiting the highest absolute E_d' magnitudes across the entire amplitude range.

3.4.3. Lissajous plots

Building upon the previous analysis of elastic modulus derived from first-order harmonics, in this section further investigated the nonlinear viscoelastic response by analyzing higher-order harmonic contributions during large amplitude deformations (Sagis & Fischer, 2014). The surface pressure and deformation relationship was characterized using Lissajous plots (Fig. 4), where the right and left sides of the y-axis represented interface compression and expansion, respectively. At 10% deformation amplitude, all systems exhibited a nearly elliptical Lissajous pattern, demonstrating that the protein-stabilized interfaces behaved in a linear viscoelastic manner at this amplitude. When the amplitude increased to 20%, all samples produced broader, asymmetric curves, revealing enhanced viscous behavior and the emergence of nonlinear viscoelastic (NLVE) characteristics (García-Moreno et al., 2021). At 20% and 30% amplitudes, the Lissajous plots exhibited a sharp increase in surface pressure at the start of expansion (lower left corner of the plots), indicating higher energy dissipation at this stage. As the interface continued to expand, the curve slope decreased, suggesting that the interfacial membrane underwent strain softening (Chutinara et al., 2024). The results demonstrate that during interfacial expansion, the droplet surface area continuously increased, leading to a reduction in interfacial protein concentration and disruption of the interfacial structure. During compression (upper right corner of the plots), the slope of the interfacial curve increased with decreasing surface area and rising interfacial protein concentration, indicating strain hardening at the interface (Ma et al., 2024). The Lissajous curves generated by CMP consistently positioned closer to the longitudinal axis compared to those of MP, indicating that CMP formed stiffer interfacial films.

3.4.4. S-factors

The nonlinear rheological response of interfacial layers was quantitatively evaluated through S-factor analysis, where S = 0 corresponded to LVE behavior, S < 0 indicated strain softening, and S > 0 signified strain hardening (García-Moreno et al., 2021). During interfacial expansion (Fig. 5A), all protein-stabilized interfaces exhibited negative S_{ext} values that became progressively more pronounced with increasing amplitude, confirming strain-softening behavior. Conversely, compressive deformation (Fig. 5B) produced positive S_{com} values across all systems, clearly demonstrating strain-hardening characteristics. The amplitude-dependent increase in S_{com} values reflected enhanced interfacial rigidity and a gradual transition toward plastic deformation during area reduction, consistent with the Lissajous plot analyses in Fig. 4.

The strain hardening plastic behavior caused emulsion fragmentation during rapid dispersion processes, while the strain softening effect facilitated interfacial stretching and emulsion formation (Zhou et al., 2025). Although CMP formed stiffer interfacial films with stronger intermolecular interactions, MP-stabilized interfaces exhibited significantly greater strain softening during expansion than CMP, indicating superior interfacial extensibility (Ravera et al., 2021). These findings suggested that trace amounts of chitin could effectively modulate oil-water interfacial behavior. This observation was consistent with the findings of O'Sullivan et al. (2016), demonstrating that residual chitin could co-adsorb with proteins at the oil-water interface, enhancing protein affinity for both phases and consequently improving the flexibility of interfacial films and overall emulsification performance. Notably, WP-stabilized interfaces maintained S-factors approaching zero across all tested conditions, indicating nearly ideal linear viscoelastic behavior and exceptional resistance to external deformations (Schröder et al., 2017). In contrast, SP-stabilized interfaces displayed marked strain hardening during expansion, reflecting their relatively brittle character and limited deformability.

3.5. Emulsion properties

3.5.1. Droplet size and ζ-potential

The emulsification performance of various proteins was systematically evaluated through the preparation and characterization of oil-in-water emulsions. Emulsion characterization revealed significant variations in droplet size distribution ($d_{4,3}$) among samples prepared with 0.5% (w/v) protein solutions (Table 2). Both MP and CMP generated substantially smaller droplets than SP and WP, correlating with their superior interfacial activity profiles observed in Fig. 2. This correlation confirmed that proteins exhibiting greater interfacial tension reduction capacity effectively lowered the energy barrier for emulsion formation, consequently promoting the generation of finer droplets (Ho et al., 2022). Interestingly, despite comparable emulsifying activity between MP and CMP, MP-stabilized emulsions approximately 5% smaller droplets than CMP. This discrepancy could not be explained by interfacial tension variations alone. Additional dilatational rheological analysis revealed that MP-stabilized interfaces displayed more pronounced strain softening behavior than CMP across all amplitudes, suggesting a reduced energy requirement for droplet formation in

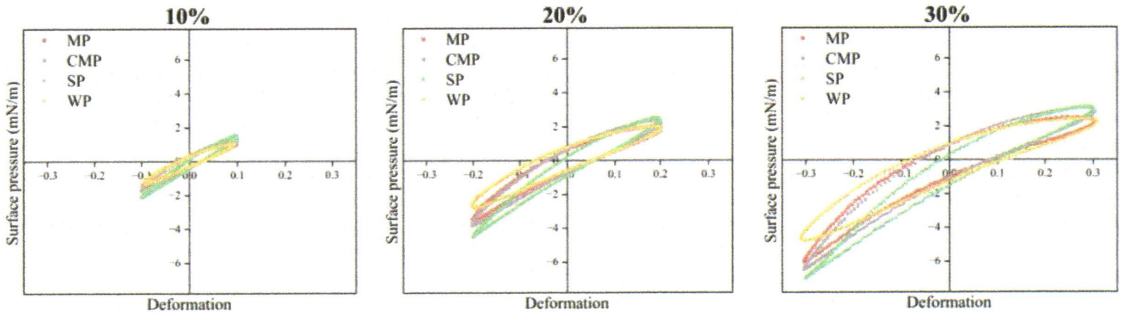

Fig. 4. Lissajous plots of oil-water interfaces stabilized by mycoprotein (MP), chitinase-treated mycoprotein (CMP), soy protein (SP) and whey protein (WP). Amplitude sweeps were set to 10%, 20%, and 30%.

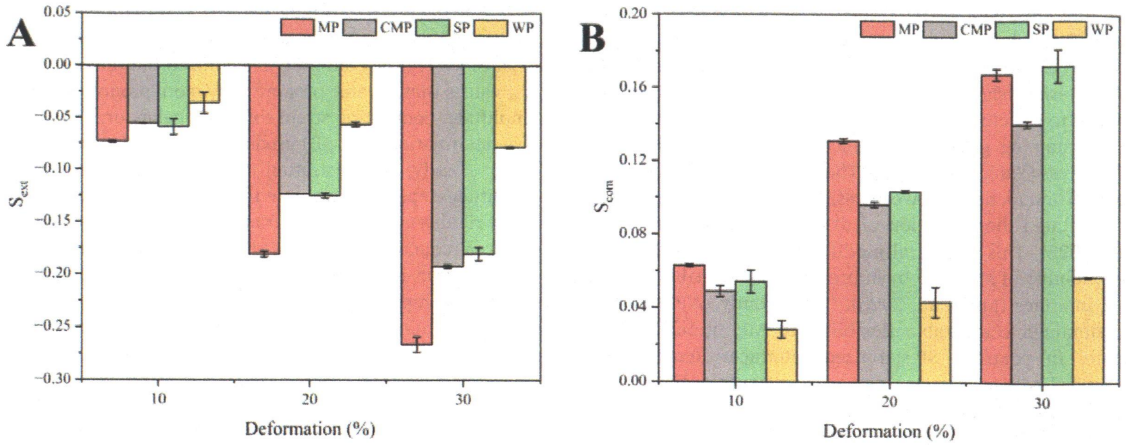

Fig. 5. S-factors calculated from expansion (A) and compression (B) of oil-water interfaces stabilized by mycoprotein (MP), chitinase-treated mycoprotein (CMP), soy protein (SP) and whey protein (WP).

Table 2
Droplet size, ζ-potential, adsorbed protein (%) and interfacial protein concentration of mycoprotein (MP), chitinase-treated MP (CMP), soy protein (SP) and whey protein (WP) -stabilized emulsions.

	MP	CMP	SP	WP
$d_{4,3}$ (μm)	0.70 ± 0.08^{b}	0.74 ± 0.06^{b}	0.91 ± 0.03^{a}	0.88 ± 0.05^{a}
ζ-potential (mV)	-39.81 ± 0.57^{c}	-36.73 ± 0.03^{b}	-32.91 ± 0.31^{a}	-41.74 ± 0.29^{d}
Adsorbed protein (%)	50.13 ± 0.19^{c}	51.71 ± 1.43^{b}	53.07 ± 1.27^{a}	49.27 ± 0.93^{c}
Γ (mg/m^2)	1.85 ± 0.00^{d}	1.95 ± 0.03^{b}	2.16 ± 0.00^{a}	1.90 ± 0.01^{c}

MP-stabilized emulsions (Zhou et al., 2025). Notably, WP-stabilized emulsions also exhibited relatively smaller droplet size, which could be attributed to the remarkable elastic response of WP interfacial films during deformation. This enhanced elasticity effectively resisted interfacial distortion and prevented droplet coalescence (Yang et al., 2024). These findings collectively demonstrated that emulsion formation involved not merely simple emulsifier diffusion, but rather complex interfacial engineering encompassing both adsorption kinetics and film stabilization mechanisms (Chutinara et al., 2024; Sagis & Fischer, 2014).

The ζ-potential exhibited a positive correlation with inter-droplet electrostatic repulsion, where increased surface charge density significantly enhanced emulsion stability (Li et al., 2021). As presented in Table 2, MP-stabilized emulsions exhibited stronger electrostatic stabilization, as evidenced by their more negative ζ-potential. This observation could be attributed to conformational changes of MP at the emulsion interface, which led to the re-exposure of internal charged groups on the protein surface (García-Moreno et al., 2021). In contrast, SP-stabilized emulsions showed no significant change in ζ-potential compared to the protein solution. Notably, WP exhibited a marked increase in ζ-potential to −41.74 mV upon emulsion formation.

3.5.2. *Interfacial adsorption of proteins*

The adsorbed interfacial layer critically governed emulsion stability by modulating aggregation resistance and flocculation behavior. As evidenced in Table 2, CMP-stabilized emulsions demonstrated significantly enhanced interfacial adsorption capacity compared to MP. This improvement likely resulted from chitin removal exposing hydrophobic domains in protein molecules, which strengthened intermolecular interactions within the interfacial layer and increased its structural density (Yuan et al., 2013). Additionally, CMP's substantially higher solubility enabled more uniform protein distribution at the oil-water interface (Yang et al., 2024). These combined effects produced a thicker, more cohesive interfacial layer. WP-stabilized emulsions showed comparatively lower protein adsorption, while SP exhibited maximal adsorption efficiency due to its outstanding solubility. However this excessive interfacial protein loading formed excessively rigid interfacial films, ultimately leading to emulsion system instability (Li et al., 2021).

3.5.3. *Storage stability*

The storage stability of protein-stabilized emulsions was evaluated through systematic monitoring of droplet size evolution over 30 d (Fig. 6). MP-stabilized emulsions maintained exceptional stability throughout storage, whereas the CMP-stabilized emulsions showed progressive droplet size enlargement, indicating pronounced droplet aggregation and flocculation during the storage period (Li et al., 2021). This distinct behavior likely stemmed from the significantly higher surface hydrophobicity of CMP compared to MP. At elevated protein concentrations, CMP underwent interfacial folding driven by hydrophobic interactions, resulting in the internalization of hydrophobic residues and consequent disruption of oil-phase contact (Xie et al., 2023). Furthermore, MP-stabilized emulsions demonstrated higher absolute ζ-potential values than CMP systems, indicating stronger electrostatic repulsion between droplets that effectively suppressed droplet coalescence (Liu et al., 2022). Complementary dilatational rheology analysis revealed that MP-interfaces displayed superior strain softening behavior, demonstrating enhanced interfacial flexibility that effectively resisted droplet flocculation and rupture during storage (Zhou et al., 2025). These characteristics collectively contributed to improved MP-stabilized emulsions stability. In comparison, SP-stabilized interfaces showed pronounced strain hardening in expansion rheology combined with relatively low absolute ζ-potential, rendering the emulsion droplets more susceptible to collision and flocculation, demonstrated the poorest storage stability (Ravera et al., 2021). Conversely, WP-stabilized interface exhibited linear viscoelastic behavior even under large deformations, while the resulting emulsion demonstrated a high absolute ζ-potential value. These combined characteristics endowed the WP-stabilized emulsion with exceptional storage stability comparable to that of MP (Yang et al., 2024).

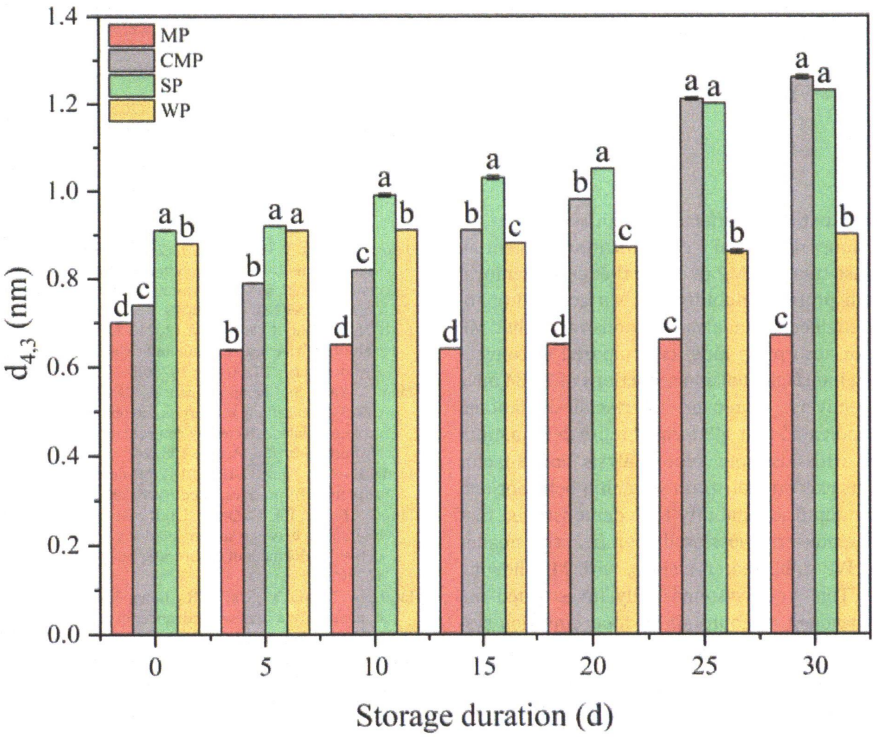

Fig. 6. Droplet size of 0.5% (w/v) emulsions stabilized by mycoprotein (MP), chitinase-treated mycoprotein (CMP), soy protein (SP) and whey protein (WP) during 30 d storage.

3.5.4. pH stability

The pH stability of protein-stabilized emulsions was evaluated by monitoring droplet size variations across pH 3.0–7.0. As shown in Fig. 7, emulsion droplet diameters exhibited progressive reduction with increasing deviation from pH 5.0. Emulsions prepared at pH 4.0–5.0 displayed partial destabilization during storage, in accordance with previous findings by Liang and Tang (2013). This phenomenon could be attributed to the fact that most proteins had isoelectric points at pH 4.0–5.0, where their solubility was significantly reduced (Grossmann & McClements, 2023). When the protein concentration was insufficient to effectively cover the oil droplet interfaces, attractive interactions between droplets could induce droplet flocculation (Lian et al., 2023). Consistent with long-term stability observations, MP-stabilized emulsions demonstrated superior pH stability compared to CMP systems. This phenomenon could be attributed to the electrostatic stabilization provided by positively charged chitin groups in MP-stabilized emulsions under acidic conditions, which effectively inhibited oil droplet aggregation. Furthermore, the chitin-protein interactions modulated the secondary structure of proteins and enhanced interfacial binding affinity, resulting in superior interfacial elastic behavior that effectively mitigated pH-induced destabilization (Yahyaei et al., 2018). Consistent with the above findings, Lv et al. (2023) demonstrated that O/W Pickering emulsions fabricated with chitin additives exhibited remarkable stability across a broad pH range. Moreover, SP-stabilized emulsions demonstrated superior pH stability compared to CMP, while showing comparable performance to MP. This phenomenon was primarily attributed to the alkaline extraction-isoelectric precipitation process employed in the preparation of MP, CMP, and SP. The process induced

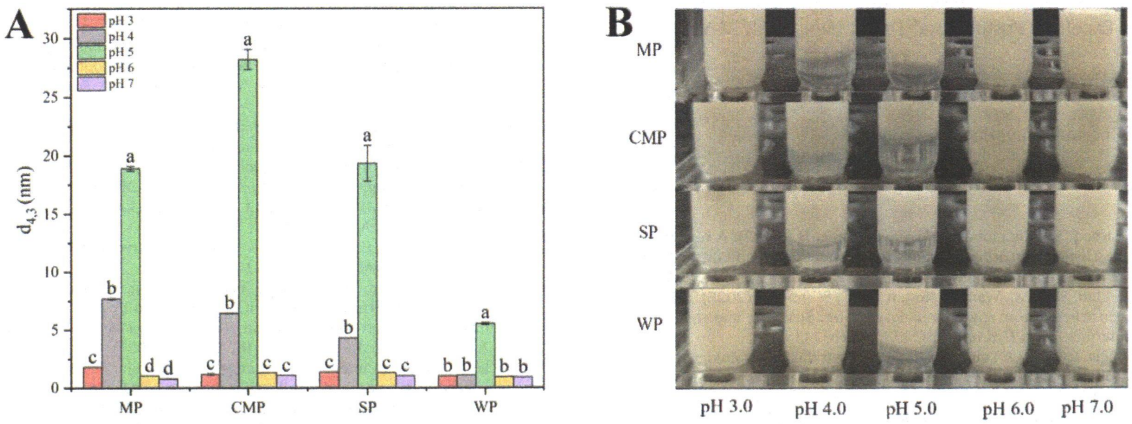

Fig. 7. (A) Droplet size of 0.5% (w/v) emulsions stabilized by mycoprotein (MP), chitinase-treated MP (CMP), soy protein (SP), and whey protein (WP) at pH 3.0–7.0. (B) Visual appearance of the corresponding emulsions at pH 3.0–7.0.

conformational changes of proteins ultimately compromised the pH stability of the protein-stabilized emulsions (Jiang et al., 2010). while WP maintained optimal stability due to its disulfide-rich structure that preserved conformational integrity near the isoelectric region (Schröder et al., 2017).

4. Conclusions

This study focused on evaluating the effects of residual chitin in MP on protein interfacial properties and emulsification potential. Comparing MP with chitinase-treated CMP revealed that chitin removal significantly enhanced both protein solubility and surface hydrophobicity. Further interfacial engineering analysis demonstrated that MP and CMP exhibited superior adsorption kinetics compared to conventional SP and WP, achieving interfacial tension reductions of 10.34 mN/m and 9.30 mN/m, respectively. Moreover, interfacial dilatational rheology characterization indicated that MP formed more deformation-resistant interfacial films, with Lissajous plot analysis and S-factor quantification confirming its exceptional strain softening behavior and enhanced film extensibility. Emulsion stability tests demonstrated that MP- and CMP-stabilized emulsions possessed significantly smaller droplet sizes than SP- and WP-stabilized emulsions, with MP showing superior stability to CMP. This study systematically investigated the application of *Fusarium venenatum* mycoprotein in food emulsion systems, providing practical guidance for its use as an alternative to conventional protein emulsifiers. The findings establish a fundamental basis for advancing mycoprotein utilization in the food industry, particularly in the development of next-generation functional food products.

CRediT authorship contribution statement

Yingying Jin: Writing – review & editing, Writing – original draft, Software, Methodology, Investigation, Conceptualization. **Hanyun Jiang:** Methodology, Investigation. **Guocheng Du:** Methodology, Investigation. **Jian Chen:** Supervision, Methodology, Conceptualization. **Zhitong Zhou:** Writing – review & editing, Supervision, Funding acquisition, Conceptualization. **Xiao Liu:** Writing – review & editing, Supervision, Funding acquisition, Conceptualization.

Declaration of competing interest

The authors declare no competing financial interest.

Acknowledgements

This research was supported by the Natural Science Foundation of Jiangsu Province (No. BK20241611), the Jiangsu Basic Research Center for Synthetic Biology (No. BK20233003), and the Jiangsu Funding Program for Excellent Postdoctoral Talent (No. 2024ZB563).

Data availability

Data will be made available on request.

References

Ahmad, M. I., Farooq, S., Alhamoud, Y., Li, C., & Zhang, H. (2022). A review on mycoprotein: History, nutritional composition, production methods, and health benefits. *Trends in Food Science & Technology, 121*, 14–29.

Cai, J., Zhang, S., Liu, S., Li, X., Wan, Z., Noskov, B. A., & Yang, X. (2025). pH-responsive microgels constructed from soy protein coacervates: Structure and rheology at the oil-water interface. *Food Hydrocolloids, 167*, Article 111433.

Chutinara, C., Sagis, L. M. C., & Landman, J. (2024). Interfacial rheological properties of pepsin-hydrolyzed lentil protein isolate at oil-water interfaces. *Food Hydrocolloids, 155*, Article 110201.

Derbyshire, E., & Ayoob, K.-T. (2019). Mycoprotein. *Nutrition Today, 54*(1), 7–15.

García-Moreno, P. J., Yang, J., Gregersen, S., Jones, N. C., Berton-Carabin, C. C., Sagis, L. M. C., Hoffmann, S. V., Marcatili, P., Overgaard, M. T., Hansen, E. B., & Jacobsen, C. (2021). The structure, viscoelasticity and charge of potato peptides adsorbed at the oil-water interface determine the physicochemical stability of fish oil-in-water emulsions. *Food Hydrocolloids, 115*, Article 106605.

Garcia-Rubio, R., de Oliveira, H. C., Rivera, J., & Trevijano-Contador, N. (2020). The fungal cell wall: Candida, cryptococcus, and aspergillus species. *Frontiers in Microbiology, 10*, 2993.

Grossmann, L., & McClements, D. J. (2023). Current insights into protein solubility: A review of its importance for alternative proteins. *Food Hydrocolloids, 137*, Article 108416.

Ho, T. M., Razzaghi, A., Ramachandran, A., & Mikkonen, K. S. (2022). Emulsion characterization via microfluidic devices: A review on interfacial tension and stability to coalescence. *Advances in Colloid and Interface Science, 299*, Article 102541.

Jiang, J., Xiong, Y. L., & Chen, J. (2010). pH Shifting alters solubility characteristics and thermal stability of soy protein isolate and its globulin fractions in different pH, salt concentration, and temperature conditions. *Journal of Agricultural and Food Chemistry, 58*(13), 8035–8042.

Li, H., Li, F., Wu, X., & Wu, W. (2021). Effect of rice bran rancidity on the emulsion stability of rice bran protein and structural characteristics of interface protein. *Food Hydrocolloids, 121*, Article 107006.

Lian, Z., Yang, S., Cheng, L., Liao, P., Dai, S., Tong, X., Tian, T., Wang, H., & Jiang, L. (2023). Emulsifying properties and oil–water interface properties of succinylated soy protein isolate: Affected by conformational flexibility of the interfacial protein. *Food Hydrocolloids, 136*, Article 108224.

Liang, H.-N., & Tang, C.-H. (2013). pH-dependent emulsifying properties of pea [Pisum sativum (L.)] proteins. *Food Hydrocolloids, 33*(2), 309–319.

Liu, G., Hu, M., Du, X., Qi, B., Lu, K., Zhou, S., Xie, F., & Li, Y. (2022). Study on the interaction between succinylated soy protein isolate and chitosan and its utilization in the development of oil-in-water bilayer emulsions. *Food Hydrocolloids, 124*, Article 107309.

Lv, J., Lv, X., Ma, M., Oh, D.-H., Jiang, Z., & Fu, X. (2023). Chitin and chitin-based biomaterials: A review of advances in processing and food applications. *Carbohydrate Polymers, 299*, Article 120142.

Ma, X., Habibi, M., & Sagis, L. M. C. (2024). Interfacial and foaming properties of soluble lupin protein isolates: Effect of pH. *Food Hydrocolloids, 155*, Article 110228.

Ma, X., Habibi, M., & Sagis, L. M. C. (2025). Air-water interfacial and foaming properties of lupin protein-polysaccharide soluble complexes: Role of physicochemical properties, morphological characteristics, and flexibility. *Food Hydrocolloids, 165*, Article 111247.

Malhotra, A., & Coupland, J. N. (2004). The effect of surfactants on the solubility, zeta potential, and viscosity of soy protein isolates. *Food Hydrocolloids, 18*(1), 101–108.

O'Sullivan, J., Murray, B., Flynn, C., & Norton, I. (2016). The effect of ultrasound treatment on the structural, physical and emulsifying properties of animal and vegetable proteins. *Food Hydrocolloids, 53*, 141–154.

Pastrana-Pastrana, Á. J., Rodríguez-Herrera, R., Solanilla-Duque, J. F., & Flores-Gallegos, A. C. (2025). Plant proteins, insects, edible mushrooms and algae: More sustainable alternatives to conventional animal protein. *Journal of Future Foods, 5*(3), 248–256.

Puljić, L., Banožić, M., Kajić, N., Vasilj, V., Habschied, K., & Mastanjević, K. (2025). Advancements in research on alternative protein sources and their application in food products: A systematic review. *Processes, 13*(1), 8–129.

Ravera, F., Dziza, K., Santini, E., Cristofolini, L., & Liggieri, L. (2021). Emulsification and emulsion stability: The role of the interfacial properties. *Advances in Colloid and Interface Science, 288*, Article 102344.

Romero, A., Beaumal, V., David-Briand, E., Cordobes, F., Guerrero, A., & Anton, M. (2011). Interfacial and oil/water emulsions characterization of potato protein isolates. *Journal of Agricultural and Food Chemistry, 59*(17), 9466–9474.

Ryan, K. N., Vardhanabhuti, B., Jaramillo, D. P., van Zanten, J. H., Coupland, J. N., & Foegeding, E. A. (2012). Stability and mechanism of whey protein soluble aggregates thermally treated with salts. *Food Hydrocolloids, 27*(2), 411–420.

Sagis, L. M. C., & Fischer, P. (2014). Nonlinear rheology of complex fluid–fluid interfaces. *Current Opinion in Colloid & Interface Science, 19*(6), 520–529.

Schröder, A., Berton-Carabin, C., Venema, P., & Cornacchia, L. (2017). Interfacial properties of whey protein and whey protein hydrolysates and their influence on O/W emulsion stability. *Food Hydrocolloids, 73*, 129–140.

Tavares, L., Souza, H. K. S., Gonçalves, M. P., & Rocha, C. M. R. (2021). Physicochemical and microstructural properties of composite edible film obtained by complex coacervation between chitosan and whey protein isolate. *Food Hydrocolloids, 113*, Article 106471.

Wang, L., Zhang, S., Jiang, W., Zhao, H., & Fu, J. (2020). Ability of casein hydrolysate-carboxymethyl chitosan conjugates to stabilize a nanoemulsion: Improved freeze-thaw and pH stability. *Food Hydrocolloids, 101*, Article 105452.

Wen, J., Zhao, J., Zhang, Y., Jiang, L., & Sui, X. (2024). Oil-water interfacial behavior of soy protein nanoparticles in high internal phase Pickering emulsion. *Food Hydrocolloids, 152*, Article 109927.

Wood, P., & Tavan, M. (2022). A review of the alternative protein industry. *Current Opinion in Food Science, 47*, Article 100869.

Xie, H., Ouyang, K., Shi, W., Wang, W., Wang, Y., Xiong, H., & Zhao, Q. (2023). Enhancing the interfacial stability of O/W emulsion by adjusting interactions of chitosan and rice protein hydrolysate. *Food Hydrocolloids, 137*, Article 108406.

Xiong, Z. Y., Yu, T., Lv, J. R., Wang, J. H., & Fu, X. (2025). Chitin nanofiber-stabilized pickering emulsion interacting with egg white protein: Structural features, interfacial properties, and stability. *Food Hydrocolloids, 161*, Article 110866.

Yahyaei, M., Mehrnejad, F., Naderi-Manesh, H., & Rezayan, A. H. (2018). Protein adsorption onto polysaccharides: Comparison of chitosan and chitin polymers. *Carbohydrate Polymers, 191*, 191–197.

Yang, J., Shen, P., de Groot, A., Mocking-Bode, H. C. M., Nikiforidis, C. V., & Sagis, L. M. C. (2024). Oil-water interface and emulsion stabilising properties of rapeseed proteins napin and cruciferin studied by nonlinear surface rheology. *Journal of Colloid and Interface Science, 662*, 192–207.

Yu, Z., Xu, Z., & Lau, D. (2014). Effect of acidity on chitin–protein interface: A molecular dynamics study. *BioNanoScience, 4*(3), 207–215.

Yuan, Y., Wan, Z.-L., Yin, S.-W., Teng, Z., Yang, X.-Q., Qi, J.-R., & Wang, X.-Y. (2013). Formation and dynamic interfacial adsorption of glycinin/chitosan soluble complex at acidic pH: Relationship to mixed emulsion stability. *Food Hydrocolloids, 31*(1), 85–93.

Zeng, B., Nilsson, K., Teixeira, P. G., & Bergenståhl, B. (2023). Study of mycoprotein extraction methods and its functional properties. *Colloids and Surfaces A: Physicochemical and Engineering Aspects, 659*, Article 130800.

Zhan, F., Chen, Y., Hu, J., Youssef, M., Korin, A., Li, J., & Li, B. (2020). Combining surface dilatational rheology and quantitative proteomics as a tool for understanding microstructures of air/water interfaces stabilized by sodium caseinate/tannic acid complex. *Food Hydrocolloids, 102*, Article 105627.

Zhou, Z., He, Y., Liu, Y., Deng, Y., Chen, J., & Liu, X. (2025). Improving the interfacial performance of pea protein via mild fractionation for enhanced lubrication behavior in plant-based emulsions. *Food Hydrocolloids, 164*, Article 111214.